Color Correction for Multi-view Images Using Relative Luminance and Chrominance Mapping Curves

Jae-Il Jung & Yo-Sung Ho

Journal of Signal Processing Systems
for Signal, Image, and Video Technology
(formerly the Journal of VLSI Signal Processing Systems for Signal, Image, and Video Technology)

ISSN 1939-8018
Volume 72
Number 2

J Sign Process Syst (2013) 72:107-117
DOI 10.1007/s11265-012-0717-z

Journal of
SIGNAL PROCESSING SYSTEMS
for Signal, Image, and Video Technology

Volume 72, No. 2, August 2013
Editor-in-Chief
S. Y. Kung

CONTENTS

Springer

ISSN 1939-8018

Available online
www.springerlink.com

Springer

J Sign Process Syst (2013) 72:107–117
DOI 10.1007/s11265-012-0717-z

Color Correction for Multi-view Images Using Relative Luminance and Chrominance Mapping Curves

Jae-Il Jung · Yo-Sung Ho

Received: 4 March 2010 / Revised: 22 October 2012 / Accepted: 7 November 2012 / Published online: 1 December 2012

Abstract In order to capture 3D scenes, a multi-view camera consisting of two or more cameras is widely used; however, color consistency among views is not guaranteed in many situations. In this paper, we design relative mapping curves with consideration of the properties of luminance and chrominance components to improve the consistency. The input images are categorized into source and reference views. We convert their color domain to the YUV color space, and estimate coefficients in the mapping curves by analyzing correspondences between the two views. After that, we generate lookup tables and convert the color distributions of the source views. From the experimental results, we confirm that our proposed method improves the visual quality of multi-view images and reduces Euclidean distances in the CIELab color space among views.

Keywords Color correction · Color inconsistency problem · Multi-view camera · Mapping curve

1 Introduction

The market of 3D images is rapidly growing by popular demand. The film production companies in Hollywood produce many different kinds of 3D films, and manufacturers combine 3D images in their new products for boost sales. In addition, the 3D images have been also applied to broadcasting systems, games, simulations and educational tools [1–3].

There are various methods to acquire 3D images such as a stereoscopic camera, computer graphics, and multi-view camera. In addition, special equipment including 3D scanners and depth cameras has been used to acquire distance information of scenes [4–8]. Among them, the multi-view camera is in the spotlight, since it allows viewers to select a viewpoint according to their preference.

At the initial stage, researchers used a single-view camera to get multi-view images instead of multiple cameras. They captured a static scene by repeatedly changing the viewpoint of the single-view camera; however this approach is not able to capture dynamic objects [9]. Therefore, they started to use multiple cameras to overcome this limitation. While multiple cameras can capture dynamic scenes, they lead new problems: geometrical errors and different color distribution among views. Such problems cause unnatural changes among views and degrade the performance of image processing on the multi-view images. Among the problems, the geometric error can be resolved by camera calibration and rectification [7].

The color of an object is affected by the radiance of an illuminant and the reflectance of the object surface. When capturing the object via a camera, we should consider an additional factor, a camera property. The camera responds to incident light based on its own properties including a shutter speed, sensor, sensitivity, and aperture. Therefore, even though we capture the same object under the same illuminant, the colors of the captured image can be varied according to the camera properties.

Since it is hard to perfectly adjust all the properties of multiple cameras as we wish, the color inconsistency among views is induced even though we use the cameras of the same kind; it is an inevitable problem.

J.-I. Jung (✉) · Y.-S. Ho
Gwangju Institute of Science and Technology (GIST), 123 Cheomdan-gwagiro, Buk-gu,
Gwangju 500-712, Republic of Korea
e-mail: jijung@gist.ac.kr
URL: http://vclab.gist.ac.kr

Y.-S. Ho
e-mail: hoyo@gist.ac.kr
URL: http://vclab.gist.ac.kr

Figure 1 The examples of the color inconsistency problem in the multi-view images.

(a) *race*

(b) *flamenco*

Figure 1 shows the examples of the color inconsistency problem in the multi-view images: the *race* and *flamenco* images. These images are standard test images of Moving picture expert group (MPEG). The color distributions among views are varied as shown in Fig. 1.

The inconsistent colors among views degrade not only the visual quality of multi-view images but also the performance of image processing. Most of the image processing algorithms have been designed under the color conservation assumption that corresponding pixels among views have similar colors. If this assumption is invalid, their performance becomes considerably degraded.

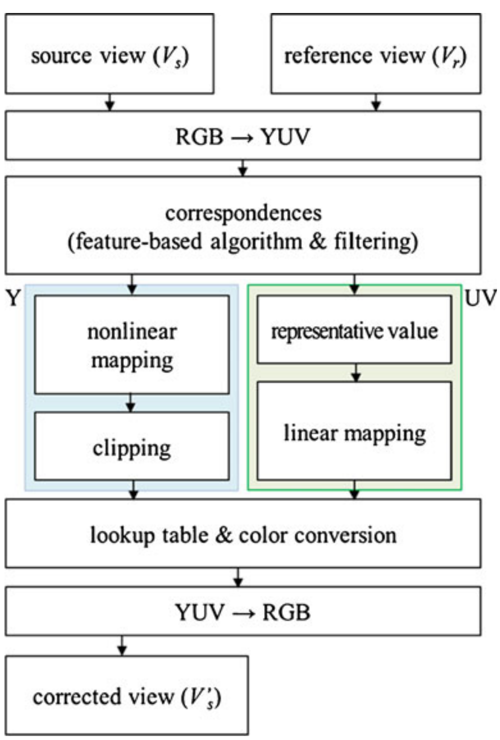

Figure 2 The flow chart of the proposed algorithm.

Therefore, color correction plays an important role in the multi-view camera system. Various algorithms have been developed to resolve the color inconsistency problem. Ilie et al. proposed a system to improve inter-camera color consistency [10]. After searching for per-camera hardware register settings, this system iteratively optimizes the settings to a known target and the average of the previous results. In addition, the system adopts software-based refinement for further improvement. Joshi et al. proposed an automatic calibrating camera arrays to achieve color consistency [11]. They iteratively adjust the camera settings to make the cameras' responses as similar as possible and calibrate residual errors in post-processing. Since the color chart is essential in both approaches, users have to capture the chart before capturing main scenes. Owing to this cumbersome task, these algorithms cannot be applied to general multi-view images which do not have the corresponding color chart images.

Alternative algorithms which automatically correct the color inconsistency without the color chart were proposed. Fecker et al. used a cumulative histogram to compare color differences among views [12]. They use histogram matching to choose the color level of a current view to each level of a reference view. In order to avoid visual artifact, they additionally handle the first and last bins in the histogram. Chen et al. also proposed a histogram-based algorithm that corrects colors with consideration of multiplicative and additive variation factors [13]. Reinhard et al. proposed a linear transformation based on a global color distribution of two

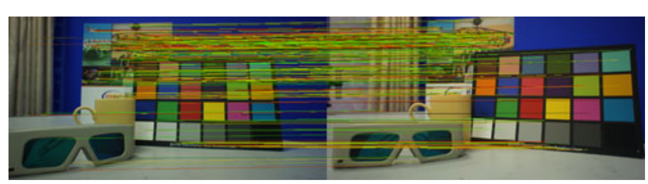

Figure 3 The result of feature-based matching.

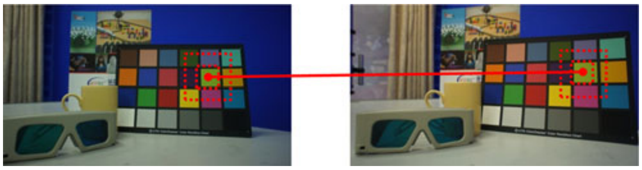

Figure 4 Additional sample acquisition by averaging neighbors with different block sizes.

input images [14]. This approach assumes the relation between the images can be described by the linear transform. Such alternative algorithms using global properties can provide reasonable results; however their performance degrades when inputs have large occlusion regions which are newly-exposed areas by viewpoint change.

In order to avoid the occlusion problem, Gangyi et al. proposed a color correction method based on region correspondences [15]. Now that they segment an image to build a statistical model, its performance depends on the result of segmentation. Yamamoto et al. introduced an energy minimization scheme via dynamic programming [16]. The energy function consists of corresponding and step-by-step terms for natural color correction. However, it is hard to determine the optimal constant coefficients in the energy function for various images, and these coefficients significantly affect its performance.

In this way, the conventional approaches have some limitations to effectively solve the color inconsistency problem. Therefore, we propose a fully automatic color correction algorithm considering the properties of occlusion regions, luminance and chrominance components.

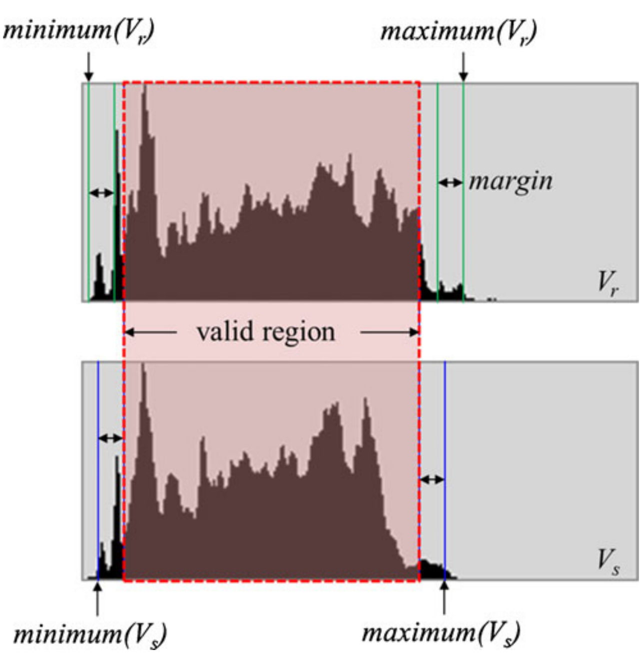

Figure 5 The valid region for inaccurate sample removal.

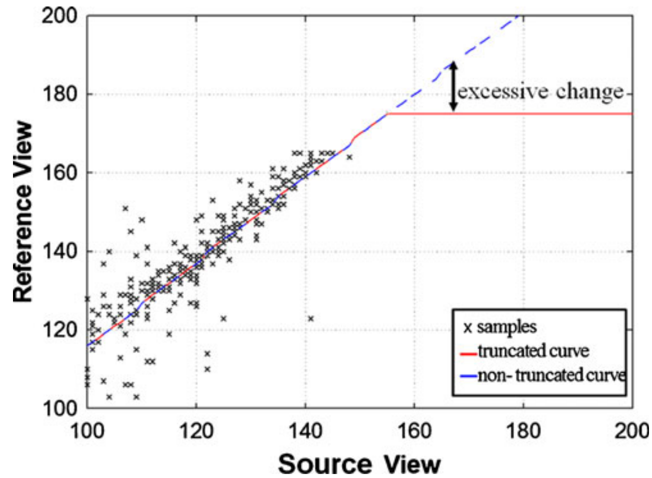

Figure 6 The initial samples and luminance mapping curve.

2 Color Correction Using Relative Mapping Curves

The proposed algorithm corrects the colors in the YUV color domain and uses different approaches for luminance and chrominance components. Figure 2 outlines the entire procedure of the proposed algorithm including correspondence extraction, mapping curve estimation, and color conversion.

At first, we categorize multi-view images into source views and a reference view. The source views are images to be corrected with consideration of the reference view. For more than two views, the center image is selected as the reference image. The following steps are independently adopted for each pair. After converting the color domain, we extract correspondences between the input images. After that we estimate optimal mapping curves for luminance and chrominance components, generate lookup tables, and convert color distribution of the source views.

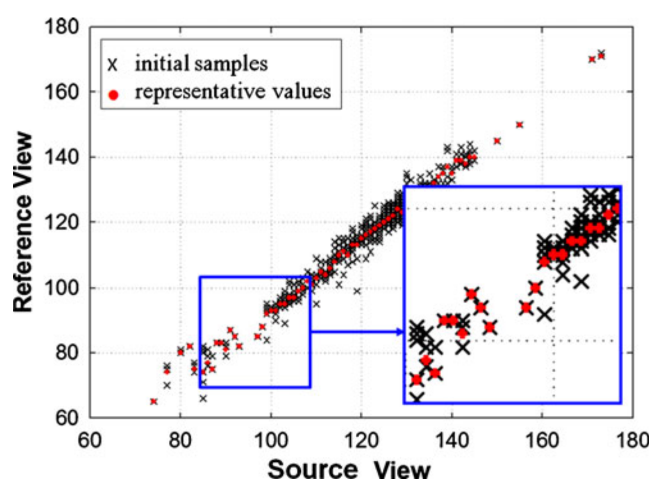

Figure 7 The initial chrominance samples and representative vales.

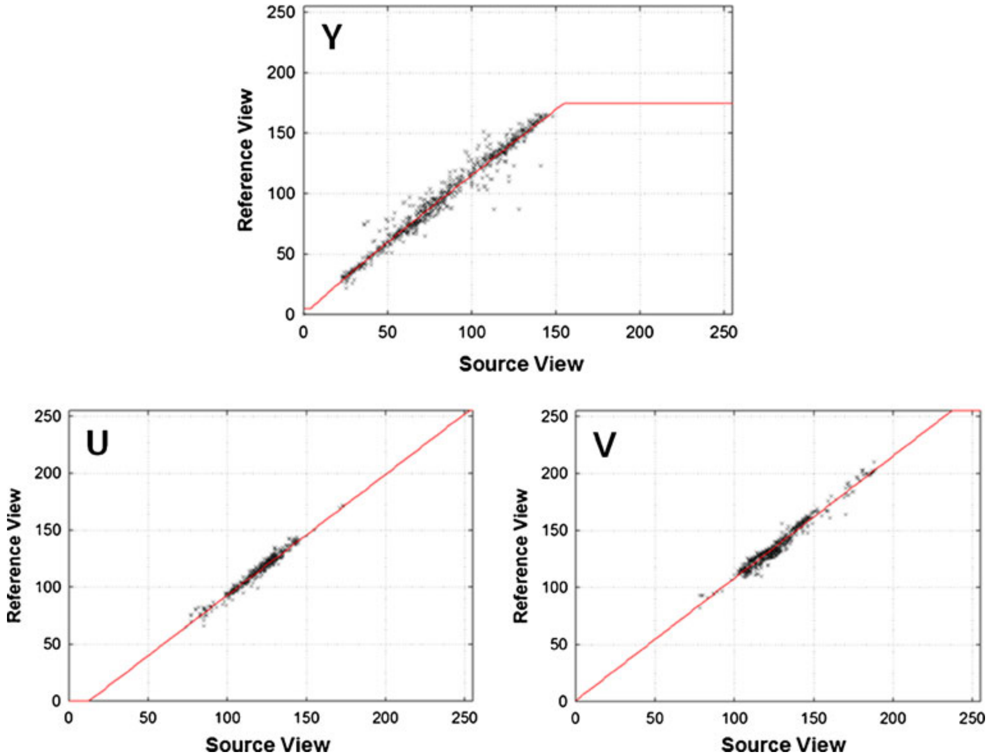

Figure 8 The initial samples and estimated mapping curves for YUV channels.

2.1 Correspondence Extraction

The proposed algorithm is based on sparse correspondences between views to avoid the occlusion problem. The co-located pixels between the views do not guarantee that one corresponds to the other, since these views are captured at different positions. The various factors including distance and camera position can affect the positions of the correspondences [17]. Many algorithms have been proposed to extract correspondences between images. Although most algorithms only use colors as a criterion, it is not appropriate for color inconsistent images. In this paper, we adopt the Scale-Invariant Feature Transform (SIFT) algorithm which is based on the appearance of the object at particular interest points and robust to image scale and rotation [18].

Figure 3 shows the results of SIFT matching. This method shows reliable results, but the number of extracted correspondences is insufficient in some cases. In addition, the extracted color values can be spoiled owing to an image noise. Therefore, we take an average of the neighbors within several local blocks as shown in Fig. 4. This method can acquire additional corresponding colors and reduce the influence of the image noise.

Now that the correspondences tend to locate around edges, unwanted pixels such as boundaries and occlusion regions can be included in the blocks. In order to reduce the influence of these pixels, we consider color distances between the current pixel and neighbors, as the bilateral filter does. It can be expressed as

$$I_b(m_0, n_0) = \sum_{m=m_0-b}^{m_0+b} \sum_{n=n_0-b}^{n_0+b} w_b(m,n) I(m,n) \tag{1}$$

where $I(m,n)$ stands for the intensity value at a point (m,n), and $I_b(m_o,n_o)$ represents the averaged value at a current point (m_o,n_o) with a block size b. $w_b(m,n)$ is an weighting factor considering the color distance and is defined as

$$w_b(m,n) = \frac{\exp\left(-\frac{\{I(m,n)-I(m_0,n_0)\}^2}{2\sigma^2}\right)}{\sum\limits_{i=m_0-b}^{m_0+b} \sum\limits_{j=n_0-b}^{n_0+b} \exp\left(-\frac{\{I(i,j)-I(m_0,n_0)\}^2}{2\sigma^2}\right)}. \tag{2}$$

In (2), the denominator is a normalization term, and the numerator is a Gaussian distribution in the intensity domain (σ=2.5). In this paper, we use three blocks of b=3, 5, and 7, and the additional samples, I_3, I_5, and I_7, are included in the correspondence set.

Table 1 The estimated coefficients and boundaries of the color mapping curves.

Coefficient	Y	U	V
Gain	1.1244	1.0868	1.0874
Offset	1.1962	-15.5793	0.4047
Gamma	0.9758	-	-
LB	3	-	-
UB	177	-	-

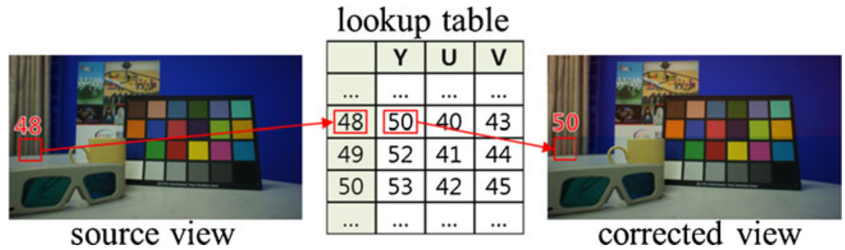

Figure 9 Color converting process using a lookup table.

Since our algorithm is based on the correspondences, the accuracy of the correspondences is very important. Especially the accuracy directly affects the mapping curves. Therefore it is required to distinguish inaccurate samples which are outside a valid region, so as to reduce the effects of image saturation or black level offset. In order to define the valid region, we calculate minimum (bottom 0.1 %) and maximum (top 0.1 %) values of the two input images by using histogram analysis. Then, we set the valid region with [*LB, UB*] where

$$\begin{aligned} LB &= \max(\mathrm{minimum}(\mathrm{V_r}), \mathrm{minimum}(\mathrm{V_s})) + \mathrm{margin} \\ UB &= \min(\mathrm{maximum}(\mathrm{V_r}), \mathrm{maximum}(\mathrm{V_s})) - \mathrm{margin} \end{aligned}. \tag{3}$$

In (3), *margin* is a constant value and is set with ten in this paper. V_r and V_s represent the reference and source views, respectively. The valid region is shown in Fig. 5. After that, we estimate luminance and chrominance mapping curves with only the samples in the valid regions

2.2 Luminance Mapping Curve

The luminance components of captured images are influenced by camera properties: gain, gamma, and offset [19]. According to them, the luminance relation between reference and source views can be modeled as

$$\begin{aligned} &Gain: && L_r = C_{gain} \times L_s \\ &Offset: && L_r = L_s + C_{offset} \\ &Gamma: && L_r = \left\{L_s / \left(2^{bitdepth} - 1\right)\right\}^{C_{gamma}} \times \left(2^{bitdepth} - 1\right) \end{aligned} \tag{4}$$

where L_r and L_s are luminance values of the reference and source views. Unlike the conventional model, C_{gain}, C_{offset}, and C_{gamma} represent relative coefficients between source and reference views. $2^{bitdepth}$ is the total number of gray levels for representing luminance component. With these relations, we design a nonlinear mapping curve for luminance correction as

$$\begin{aligned} L_r = f\left(\overline{C}, L_s\right) = C_{gain}\left\{L_s / \left(2^{bitdepth} - 1\right)\right\}^{C_{gamma}} \\ \times \left(2^{bitdepth} - 1\right) + C_{offset} \end{aligned} \tag{5}$$

where $\overline{C}$ is the vector of the coefficients. We estimate the coefficients via an outlier-removed nonlinear regression based on the Levenberg-Marquardt algorithm [20].

This process has two steps: coefficient estimation and outlier removal. In order to remove outliers, we estimate

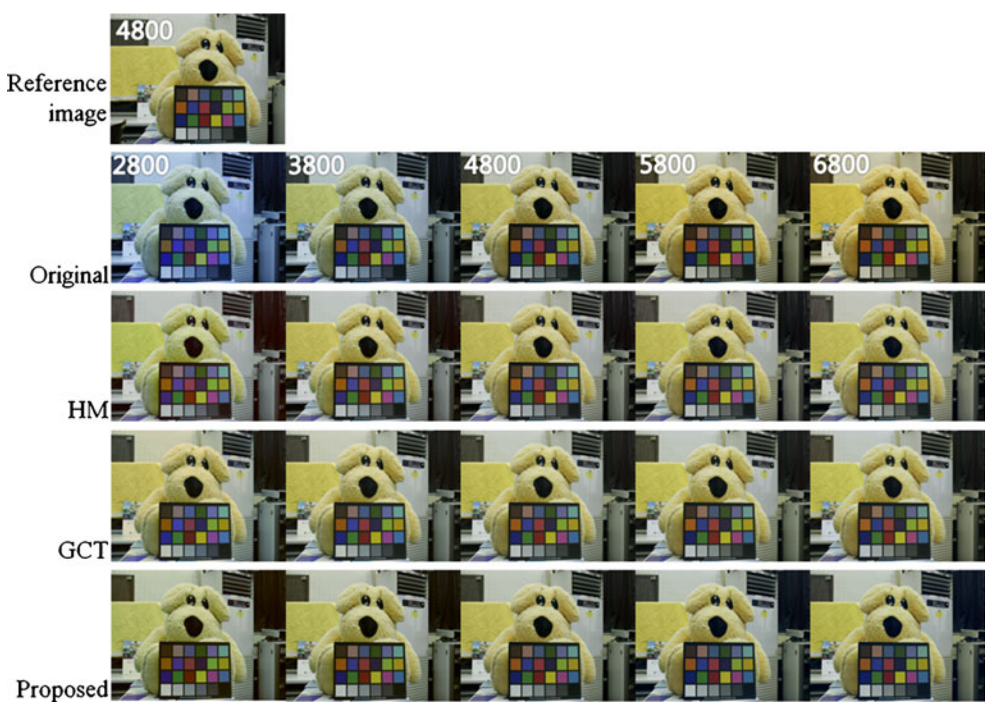

Figure 10 Visual quality comparison for various color temperature.

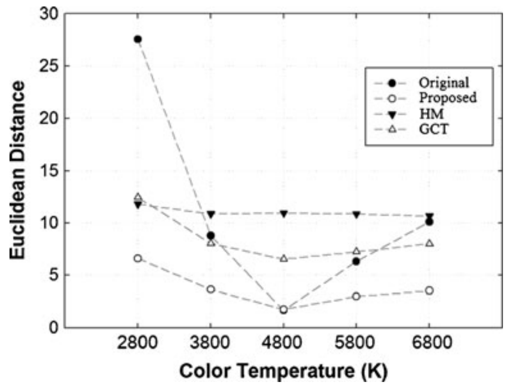

Figure 11 The Euclidean distances for various color temperature.

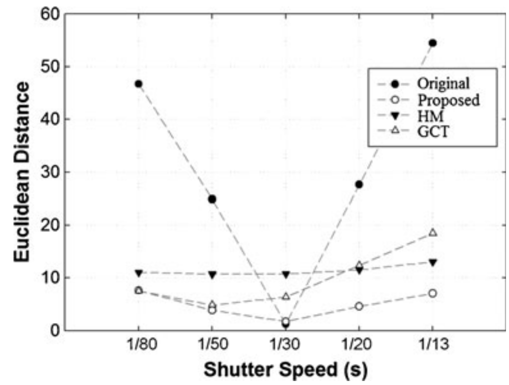

Figure 13 The Euclidean distances for various shutter speeds.

coefficients with the initial correspondences and discard the correspondences located outside doubled standard deviations from the mean value of errors. After that, we estimate coefficients again with the refined samples. This cycle is repeated until every sample is in the doubled standard deviations.

According to the estimated coefficients, (5) can generate greater intensity values than *maximum(V_r)* and smaller values than *miminum(V_r)*. Since these values cause excessive color changes in the corrected view, we truncate L'_s as

$$L'_s = \min\left(\mathrm{maximum}(\mathrm{V_r}),\ \max\left(\mathrm{minimum}(\mathrm{V_r}), \mathrm{f}\left(\overline{\mathrm{C}}, \mathrm{L_s}\right)\right)\right). \tag{6}$$

Figure 6 shows the initial samples and estimated mapping curve for the luminance component. This curve limits that the all values of the corrected view are in [*maximum(V_r)*, *minimum(V_r)*].

2.3 Chrominance Mapping Curve

Unlike the luminance case, chrominance values linearly change according to the sensor property of color temperature. Therefore we design a linear mapping curve for the chrominance components as

$$Ch_r = C_{gain} \times Ch_s + C_{offset} \tag{7}$$

where Ch_r and Ch_s are chrominance values of the reference and source views. This curve is also optimized via the least square method with outlier removal.

However, if we use the same weight for every sample during optimization as we did for estimating the luminance mapping curve, the accuracy of border chrominance values is degraded; since most chrominance values are generally concentrated around the middle as shown in Fig. 7.

Figure 12 Visual quality comparison for various shutter speeds.

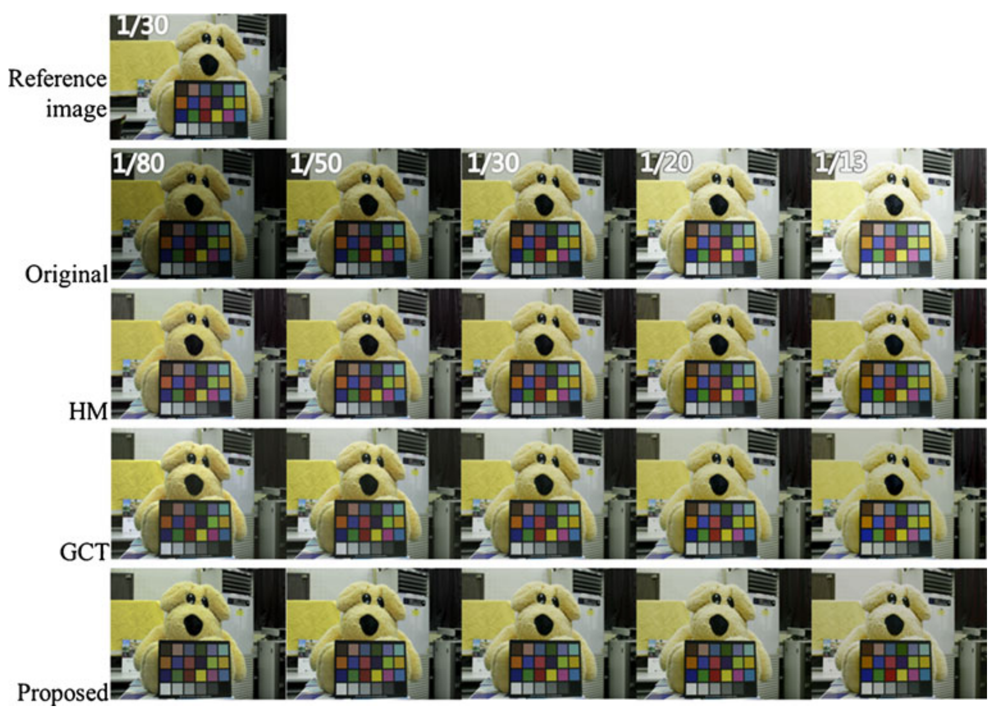

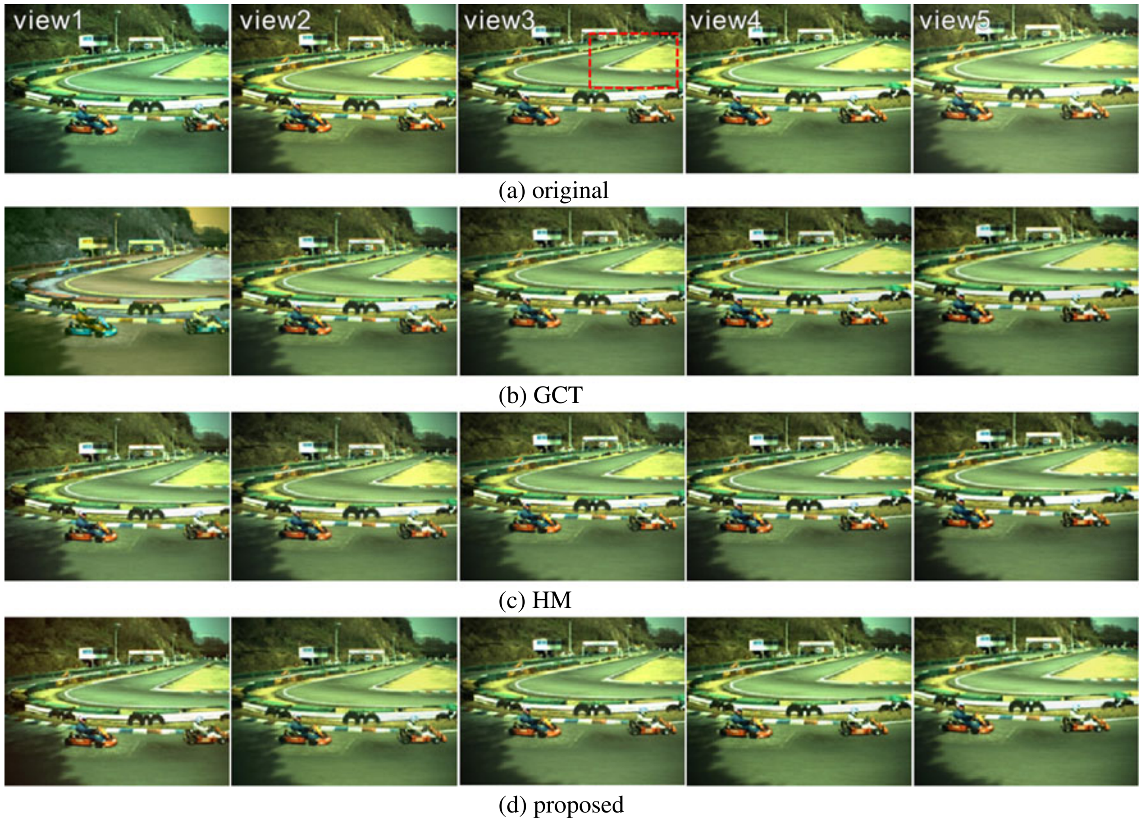

Figure 14 The results of color correction on the *race* image.

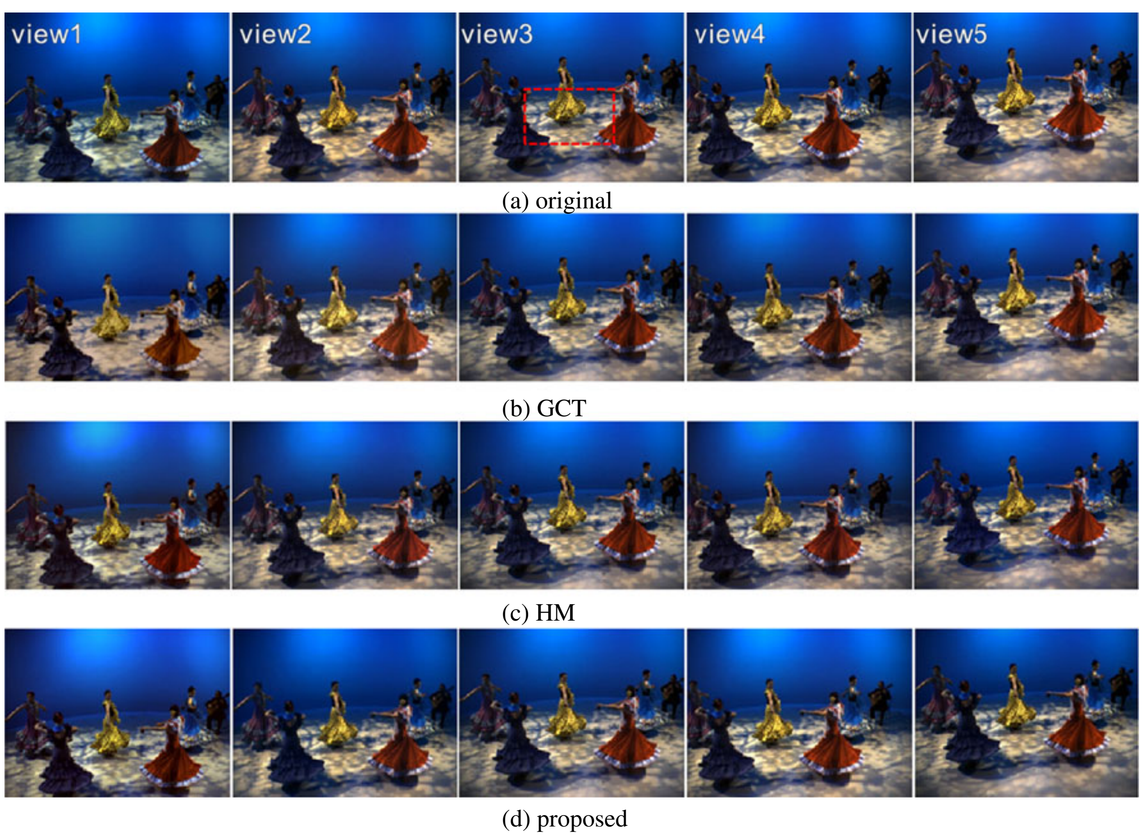

Figure 15 The results of color correction on the *flamenco* image.

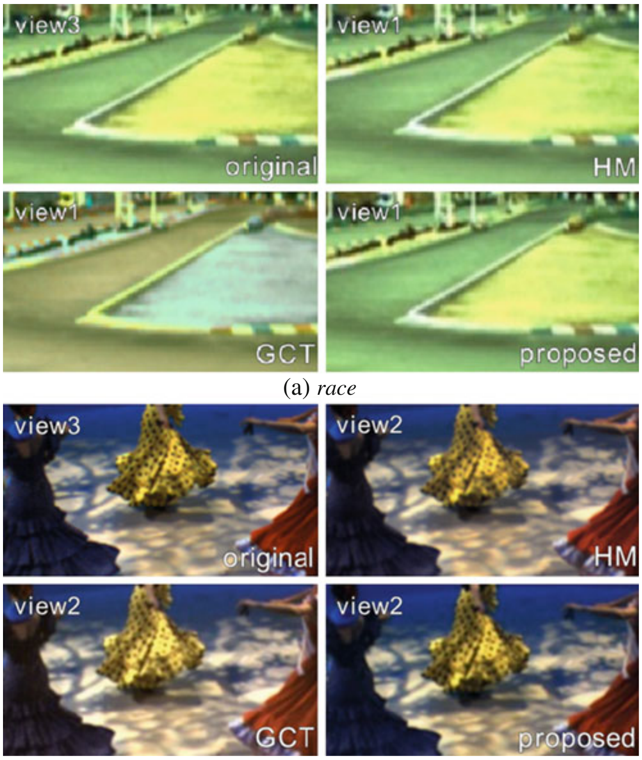

(a) *race*

(b) *flamenco*

Figure 16 The enlarged textures of the *race* and *flamenco* images.

In order to evenly distribute weight to all bins, we calculate one representative value per each bin of the source view. To this end, we discard the samples of the top 10 % and bottom 10 % in the same bin, average remainders, and set this value as a representative value of the bin. In Fig. 7, the red circles and black crosses mean the representative values and initial samples, respectively. The final mapping curve is optimized from these representative values, and the two curves are individually estimated for U and V components.

Figure 8 shows the estimated mapping curves and initial samples for YUV channels, and Table 1 shows the estimated coefficients for each channel. From the coefficients, we can quantitatively know the relative differences of color distribution between the views.

2.4 Lookup Table and Conversion

With these mapping curves, the color values of the source view are converted. However, since the corrected values have to be calculated for every pixel and every channel, this process takes a long time. To reduce the computational complexity, we generate three lookup tables for the luminance and chrominance components. The lookup tables contain pixel values to be corrected in the source view and their corrected values.

Figure 9 demonstrates an example of conversion using the lookup table. We read the luminance value (48) from the source image and find this value (48) in the lookup table. The pixel value is converted from the original value (48) to

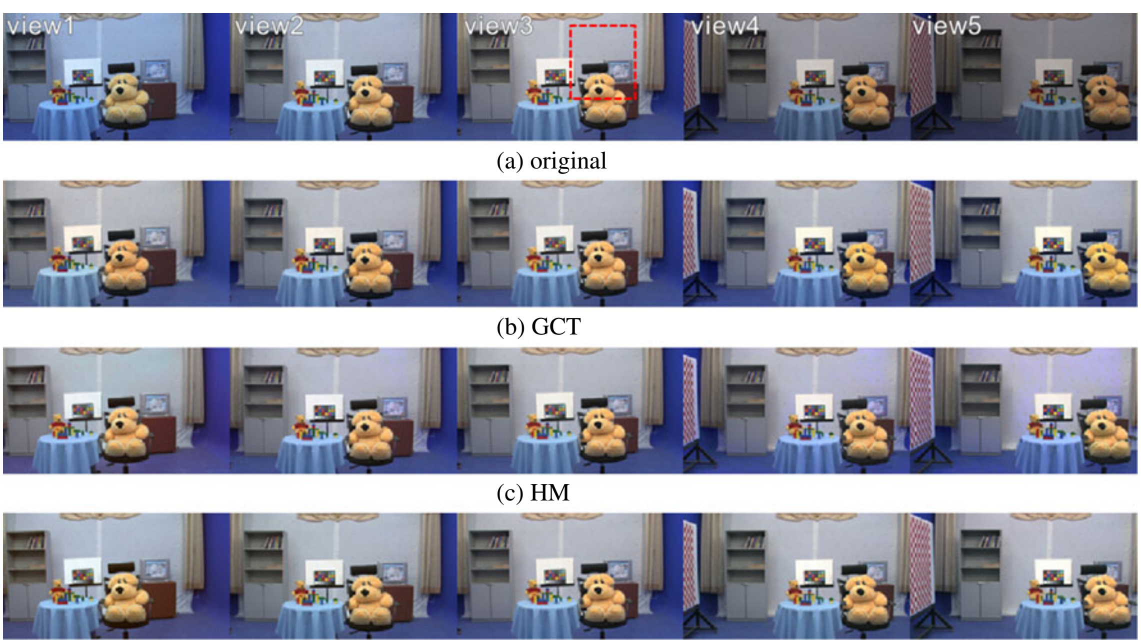

(a) original

(b) GCT

(c) HM

(d) proposed

Figure 17 The results of color correction on the severely distorted images.

Figure 18 The enlarged textures of the severely distorted images.

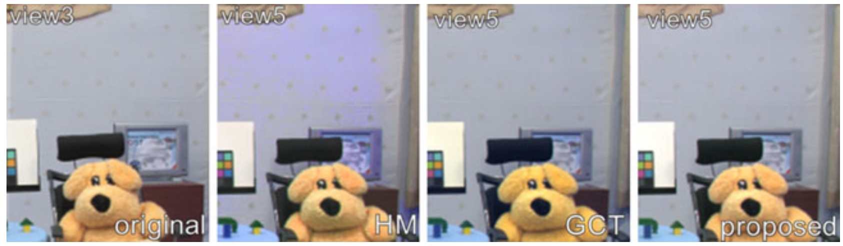

the corrected value (50). This process is conducted for all pixels and channels. After that, we can get the corrected image having similar color distribution to the reference image's one.

3 Experimental Results and Analysis

In order to evaluate the performance of the proposed algorithm, we experimented on various test images. The first experiment assesses the performance on two images captured by the same camera with different settings: color temperature and shutter speed. We implemented the histogram matching (HM) [12] and global color transfer (GCT) [14], and compared our algorithm with them. Figure 10 shows the results of color correction with respect to the different color temperature settings from 2800 K to 6800 K. The reference view was captured with 4800 K. To check how well algorithms operate when input images have consistent colors, we included the source image captured with 4800 K in the test set. For an objective evaluation, we extracted 24 values of the color chart from the reference and source views and calculated Euclidean distances in the CIELab color domain by

$$ED = \frac{1}{24}\sum_{i=1}^{24}\sqrt{\left(L_s(i) - L_r(i)\right)^2 + \left(a_s(i) - a_r(i)\right)^2 + \left(b_s(i) - b_r(i)\right)^2} \quad (8)$$

where i is the sample number of the color chart. The CIELab is a standardized color space which is designed to be perceptually linear and the Euclidean distance in the CIELab color domain is linearly related to human perception.

As shown in Figs. 10 and 11, the performances of HM and GCT are stable but lower than ours. The proposed algorithm shows the best output quality. In addition, while other algorithms severely distort the color consistent images (4800 K), our method provides reliable results.

We additionally experimented on images captured with different exposure settings, and the results are demonstrated in Figs.12 and 13. The overall tendency is similar to the previous test. In this result, GCT provides the unstable performance as the source views become brighter. From these two experiments, it is known that the proposed algorithm shows the best and stable performance for various capturing conditions.

Table 2 Comparison of Euclidean distance for original images and the results of HM, GCT, and the proposed.

Euclidean distance	Channel	View1	View2	View3	View4
Original	L	6.71	2.46	25.83	41.25
	a	5.54	1.38	4.21	6.96
	b	8.54	2.54	3.54	6.88
	all	12.57	4.09	26.63	42.81
HM	L	2.29	1.67	5.25	6.83
	a	1.50	2.21	4.25	4.33
	b	2.46	2.88	4.08	4.38
	all	4.14	4.38	8.64	10.13
GCT	L	5.33	2.58	3.33	4.50
	a	2.29	1.17	3.21	4.71
	b	2.75	1.63	4.58	6.25
	all	6.89	3.73	6.91	9.58
Proposed	L	2.21	0.96	1.38	1.67
	a	1.25	0.88	1.33	1.00
	b	3.38	1.38	1.21	1.21
	all	4.62	2.30	2.65	2.80

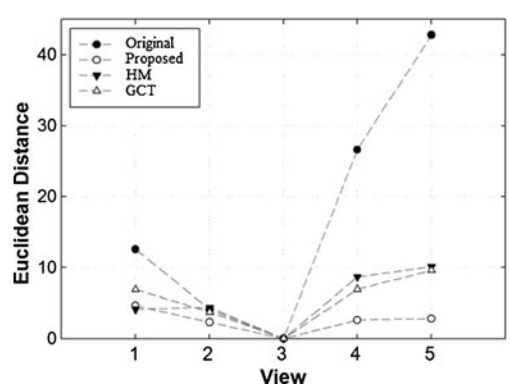

Figure 19 The Euclidean distances of color correction on severely distorted images.

We applied the proposed algorithm to the standard MPEG test images: *race* and *flamenco*. Figures 14 and 15 demonstrate the results. For close observation, we enlarged the some parts (red box) and their corresponding regions, and attached them in Fig. 16. Since these images have small occlusion regions and the colors of the occlusion regions are similar, all algorithms show reliable results; however, GCT generates excessive colors in some views.

In order to objectively evaluate each algorithm, we captured multi-view images by using five cameras with different settings. Figure 17(a) shows the original multi-view images. Figure 17(b) and (c) represent the results of HM and GCT, respectively. For close observation, we also enlarged the background region (red box) and their corresponding regions, and attached them in Fig. 18. Unlike the results of the MPEG images, the background region of HM becomes blue as the red board appears in view4 and view5.

Table 2 summarizes the comparison of Euclidean distance and Fig. 19 displays them in a diagram. From all the experimental results, it is known that the performances of HM and GCT highly depend on the property of input images, but the proposed algorithm provides the stable performance. In addition, the Euclidean distances between the reference and corrected source views of the proposed algorithm are significantly lower than those of others. It means that our method can effectively correct the color inconsistency problem.

4 Conclusions

In this paper, we have proposed a color correction algorithm based on the relative mapping curves for luminance and chrominance components. We use the feature-point based matching and outlier removal techniques to get accurate correspondences. With the correspondences, the optimal mapping curves are automatically estimated. After that, we generate lookup tables and convert the color distributions of the source views. For evaluating the proposed algorithm, we experimented on various test images, and we confirm that our proposed method improves visual quality and reduces Euclidean distances in the CIELab color space among views. The proposed method can be expected to be widely applied to multi-view image capturing and processing systems.

Acknowledgements This research is supported by Ministry of Culture, Sports and Tourism(MCST) and Korea Creative Content Agency (KOCCA) in the Culture Technology(CT) Research & Development Program 2012.

References

1. Kubota, A., Smolic, A., Magnor, M., Tanimoto, M., Chen, T., & Zhang, C. (2007). Multi-view imaging and 3DTV (special issue overview and introduction). *IEEE Signal Processing Magazine, 24*(6), 10–21.
2. Smolic, A., Mueller, K., Merkle, P., Fehn, C., Kauff, P., Eisert, P., et al. (2006). 3D video and free viewpoint video - technologies, applications and MPEG standards. *IEEE International Conference on Multimedia and Expo,* 2161–2164.
3. Tanimoto, M. (2006). Overview of free viewpoint television. *Signal Processing: Image Communication, 21*(6), 454–461.
4. Bernardini, F., & Rushmeier, H. (2002). The 3D model acquisition pipeline. *Computer Graphics Forum, 21*(2), 149–172.
5. Scharstein, D., & Szeliski, R. (2003). High-accuracy stereo depth maps using structured light. *IEEE Conference on Computer Vision and Pattern Recognition*, 195–202.
6. Gokturk, S. B., Yalcin, H., & Bamji, C. (2004). A Time-of-flight depth sensor - system description, issues and solutions. *IEEE Conference on Computer Vision and Pattern Recognition*, 35–35.
7. Kang, Y. S., & Ho, Y. S. (2011). An efficient image rectification method for parallel multi-camera arrangement. *IEEE Transactions on Consumer Electronics, 57*(3), 1041–1048.
8. Lee, E. K., & Ho, Y. S. (2011). Generation of high-quality depth maps using hybrid camera system for 3-D video. *Journal of Visual Communication and Image Representation, 22*(1), 73–84.
9. Levoy, M., & Hanrahan, P. (1996). Light field rendering. *SIGGRAPH*, 33–42.
10. Ilie, A., & Welch, G. (2005). Ensuring color consistency across multiple cameras. *IEEE International Conference on Computer Vision, II*, 1268–1275.
11. Joshi, N., Wilburn, B., Vaish, V., Levoy, M. & Horowitz, M. (2005). Automatic color calibration for large camera arrays. *UCSD CSE Technical Report*, CS2005-0821.
12. Fecker, U., Barkowsky, M., & Kaup, A. (2008). Histogram-based prefiltering for luminance and chrominance compensation of multiview video. *IEEE Transactions on Circuits and Systems for Video Technology, 18*(9), 1258–1267.
13. Chen, Y., Chen, J., & Cai, C. (2006). Luminance and chrominance correction for multi-view video using simplified color error model. *Picture Coding Symposium*, 2–17.
14. Reinhard, E., Adhikhmin, M., Gooch, B., & Shirley, P. (2001). Color transfer between images. *IEEE Computer Graphics and Applications, 21*(5), 34–41.
15. Jiang, G., Shao, F., Yu, M., Chen, K., & Chen, X. (2006). New color correction approach to multi-view images with region correspondence. *Lecture Notes in Computer Science, 4113*, 1224–1228.
16. Yamamoto, K., Kitahara, M., Kimata, H., Yendo, T., Fujii, T., Tanimoto, M., et al. (2007). Multiview video coding using view interpolation and color correction. *IEEE Transactions on Circuits and Systems for Video Technology, 17*(11), 1436–1449.
17. Hartley, R., Zisserman, A., & ebrary, I. (2003). *Multiple view geometry in computer vision* Cambridge University Press.
18. Lowe, D. (2004). Distinctive image features from scale-invariant keypoints. *International Journal of Computer Vision, 60*(2), 91–110.

19. Berns, R. S., Motta, R. J., & Gorzynski, M. E. (1993). CRT colorimetry. Part I: theory and practice. *Color Research & Application, 18*(5), 299–314.
20. Gill, P. E., & Murray, W. (1978). Algorithms for the solution of the nonlinear least-squares problem. *SIAM Journal on Numerical Analysis, 15*(5), 977–992.

Jae-Il Jung received his B.S. degree in electronics and communications engineering in 2005, and M.S degree in information display engineering from Hanyang University, Korea, in 2007. He is pursuing a Ph.D. degree in the School of Information and Communications at the Gwangju Institute of Science and Technology (GIST). His research interests include digital signal processing, 3D image processing, video coding, and digital holography.

Yo-Sung Ho received both B.S. and M.S. degrees in electronic engineering from Seoul National University, Korea, in 1981 and 1983, respectively, and Ph.D. degree in Electrical and Computer Engineering from the University of California, Santa Barbara, in 1990. He joined the Electronics and Telecommunications Research Institute (ETRI), Korea, in 1983. From 1990 to 1993, he was with Philips Laboratories, Briarcliff Manor, New York, where he was involved in development of the advanced digital high-definition television (AD-HDTV) system. In 1993, he rejoined the technical staff of ETRI and was involved in development of the Korea direct broadcast satellite (DBS) digital television and high-definition television systems. Since 1995, he has been with the Gwangju Institute of Science and Technology (GIST), where he is currently a professor in the School of Information and Communications. His research interests include digital image and video coding, image analysis and image restoration, advanced coding techniques, digital video and audio broadcasting, 3D television, and realistic broadcasting.